Structural study of the close-packed two-dimensional phases of Pb on Ge(111) and Si(111)

L. Seehofer, G. Falkenberg, D. Daboul, and R.L. Johnson

II. Institut für Experimentalphysik, Universität Hamburg, Luruper Chaussee 149, D-22761 Hamburg,
Federal Republic of Germany

The close-packed two-dimensional structures of Pb on Ge(111) and Si(111) have been studied with scanning tunneling microscopy (STM), reflection high-energy electron diffraction, and low-energy electron diffraction. Several closely-related commensurate and incommensurate phases were observed. For both adsorbate systems schematic phase diagrams are derived and compared to the predictions of the domain-wall theory for commensurate-incommensurate phase transitions. A complex structural model is presented, which describes the various incommensurate phases and is in good agreement with the STM data.

I. INTRODUCTION

Ordering in two dimensions (2D) is of great fundamental interest in science.[1,2] Most experimental realizations of 2D systems are not truly two dimensional, as is the case for a free-standing layer of atoms, but should rather be called quasi-two-dimensional[3] since they consist of a 2D layer of particles, which is not free but supported by a substrate. For these kinds of systems it is a central question how the periodicity of the quasi-2D layer relates to the periodicity of the substrate. Phase transitions between commensurate and incommensurate superstructures have attracted considerable attention over the past few years both experimentally and theoretically.[1–4]

Most of the experimental work so far has been performed on physisorbed systems such as rare gases on graphite, which have been studied with a variety of experimental techniques such as x-ray diffraction and helium atom scattering.[2,4] However, since it is predicted theoretically that these phase transitions are associated with local inhomogeneities it is highly desirable to investigate such phenomena directly in real space. Physisorbed rare gases on graphite can only be investigated at low temperatures, which makes scanning tunneling microscopy (STM) measurements more difficult. We have found that the unreactive metal-semiconductor adsorbate systems Pb on Ge(111) and Pb on Si(111) are both a kind of prototype system for investigating the local phenomena associated with commensurate-incommensurate (CI) phase transitions directly in real space with atomic resolution.

The 2D phase diagrams of Pb on Ge(111) and Si(111) have several similarities. Both systems form two different $(\sqrt{3} \times \sqrt{3})R30°$ reconstructions (in the following referred to as $\sqrt{3}$) depending on the coverage. The dilute $\sqrt{3}$ reconstructions have been shown to consist of a mixture of Pb and semiconductor adatoms both occupying T_4 sites.[5–8] Surface x-ray diffraction[9–11] (SXRD) and low-energy electron-diffraction (LEED) measurements[12] revealed that the dense phase of Pb on Si(111) is incommensurate while the dense phase of Pb on Ge(111)

is usually commensurate. Both dense phases undergo a $\sqrt{3} \leftrightarrow (1 \times 1)$ phase transition on heating and this phase transition has been attributed to a 2D melting process.[13,14] Recently it has been shown with STM that Pb on Ge(111) also forms an incommensurate phase[8] at coverages slightly above the saturation coverage of the dense $\sqrt{3}$ phase. This paper is intended to give a comprehensive overview of the various densely packed room-temperature 2D phases of Pb on Ge(111) and Si(111). Special emphasis will be given to results on the incommensurate phases of Pb on Si(111).

II. EXPERIMENT

The experiments were performed in an UHV system (base pressure $< 2 \times 10^{-11}$ mbar) consisting of a molecular-beam-epitaxy deposition chamber equipped with a reflection high-energy electron-diffraction (RHEED) apparatus, sample heating and a quartz film-thickness monitor, a separate preparation chamber for sputtering and annealing to clean the substrates, and an analysis chamber containing a LEED system and a commercial STM (OMICRON Vakuumphysik GmbH). For the STM measurements, we used electrochemically etched tungsten tips, which were formed *in situ* by scanning at high bias voltage and tunneling current. If not otherwise mentioned, all images shown here are unfiltered raw data with a linear background subtracted. The substrates were prepared using standard techniques. Prior to Pb deposition, the quality of the substrate was checked carefully with LEED, RHEED, and STM. Pb was evaporated from an effusion cell with a PBN crucible at a rate of $\sim 5 \times 10^{-3}$ ML/s where 1 ML corresponds to 7.22×10^{14} atoms/cm^2 for Ge and 7.83×10^{14} atoms/cm^2 for Si. During deposition, the pressure was maintained at less than 1×10^{-10} mbar. We found that samples could be cleaned for reuse either by sputtering and annealing (for Ge) or by simply heating up to 500 °C (for Ge and Si) to desorb all of the Pb.

III. RESULTS

A. Pb on Ge: Commensurate-incommensurate phase transition

The driving force for a CI phase transition arises from the competition between the adatom-adatom and the adatom-substrate interactions. It was shown by Frank and Van der Merwe as long ago as 1949 that in 1D the ground state of an adlayer with a density close to the commensurate value consists of broad commensurate domains separated by narrow regions, which carry the missing or additional mass.[15] These small regions can be described as solitons, domain walls, or discommensurations. The domain-wall theory of CI phase transitions in 2D predicts the existence of different kinds of domain-wall networks.[16,17] The topology of these networks depends on the symmetry of the system and on the number P of possible subdomains of the adsorbate superstructure. Generally any $(N \times M)$ superstructure has $P = NM$ equivalent subdomains, which gives $P = 3$ for a $(\sqrt{3} \times \sqrt{3})R30°$ reconstruction. For a hexagonal system with three subdomains, Bak and co-workers predicted two possible kinds of domain-wall networks depending on the energy of domain-wall crossings, namely a striped incommensurate phase (SIC) of parallel domain walls and a hexagonal incommensurate phase (HIC).[16,17]

The commensurate $\sqrt{3} - \beta$ phase of Pb on Ge(111) has been studied with a variety of experimental techniques. Surface x-ray diffraction measurements[9] and a dynamical LEED $(I\text{-}V)$ analysis[12] lead to a structural model for the commensurate Ge(111)$\sqrt{3}\beta$-Pb phase, which is similar to that originally proposed for the densely packed $\sqrt{3}$ phase of Pb on Si(111) by Estrup and Morrison.[18] It contains four Pb atoms per $\sqrt{3}$ unit cell and corresponds to a 30° rotated slightly compressed Pb(111) layer. In STM topographs of this structure, usually one protrusion per $\sqrt{3}$ unit cell can be observed (see Fig. 1). However, by changing the bias voltage and the tunneling current, also patterns with three or four maxima per $\sqrt{3}$ unit cell can be obtained. It has been shown that none of these patterns can be directly related to the positions of the Pb atoms.[19] Therefore, STM data alone are not
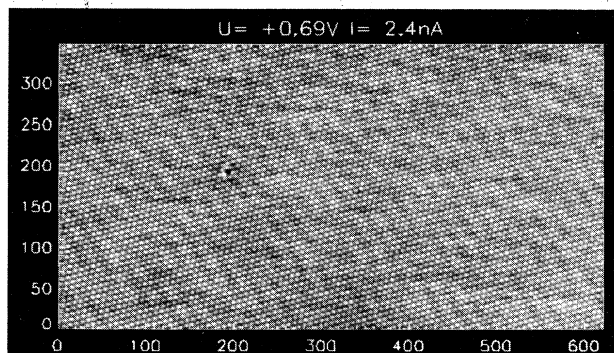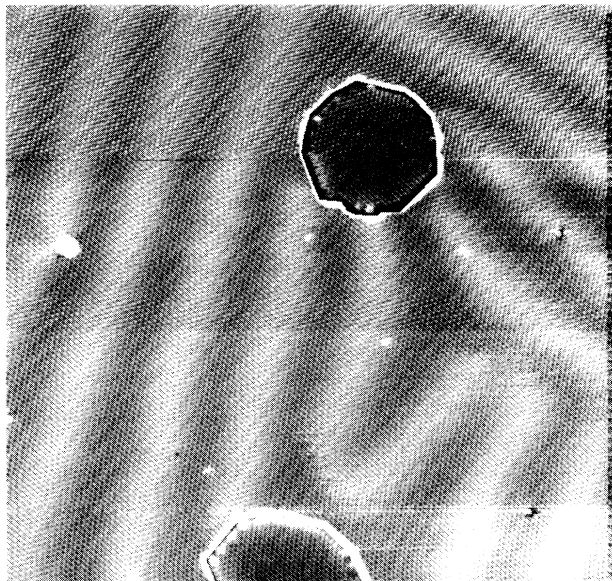

FIG. 2. STM topograph acquired at +1.5-V sample bias and 1.5-nA tunneling current from a 800×800 Å^2 area of the striped incommensurate phase of Pb on Ge(111).

sufficient to decide directly between different structural models. On well-oriented samples, we obtained almost defect-free domains of the $\sqrt{3} - \beta$ phase extending over several thousand Å. Very rarely we observed antiphase domain boundaries in these $\sqrt{3} - \beta$ reconstructed domains.

Adding a small amount of lead (~ 0.2 ML) to a saturated $\sqrt{3} - \beta$ phase introduces a drastic change in the corresponding STM topographs and the surface structure becomes incommensurate. In Fig. 2, a network of domain walls can be observed on the lower terrace, which appear as bright stripes with a width of ~ 66 Å. In agreement with the domain-wall theory for the CI phase transitions, we conclude that these domain walls carry the excess Pb density above the commensurate value. Since the domain walls run mostly parallel, the structure in Fig. 2 can be identified as a slightly distorted striped incommensurate phase. The S-shaped domain wall in the lower right corner of Fig. 2 illustrates that the domain walls are repelled by step edges as well as other domain walls. We did not observe any movement of the domain-wall lattice on the time scale of hours at room temperature, which indicates that the domain walls are pinned by the substrate. This results from the discreteness of the overlayer as shown theoretically by Pokrovsky.[20,21] On surfaces that had defects we observed more domain-wall intersections, which indicates that the domain walls can also be pinned by defects. The pinning prevents the development of a well-ordered parallel domain-wall superlattice and gives rise to the formation of domain-wall crossings instead. The height of the two small islands in Fig. 2 corresponds to the distance between two Ge(111) double layers. The islands shown are covered with the ordinary β phase, but at higher coverage we also observed similar islands cov-

FIG. 1. STM topograph of the commensurate Ge(111)$\sqrt{3} - \beta$-Pb phase.

ered with the striped phase

In high-resolution STM images, the domain walls have a rather complex appearance. Figures 3(a) and 3(b) show two STM images of the same area of the sample taken under different tunneling conditions. In Fig. 3(a), the domain walls (W) appear as bright stripes and it is easy to spot the phase shift (S) between the neighboring commensurate domains. The presence of this phase shift is in good agreement with domain-wall theory, which predicts

(a)   V= +1mV I= 1.7nA
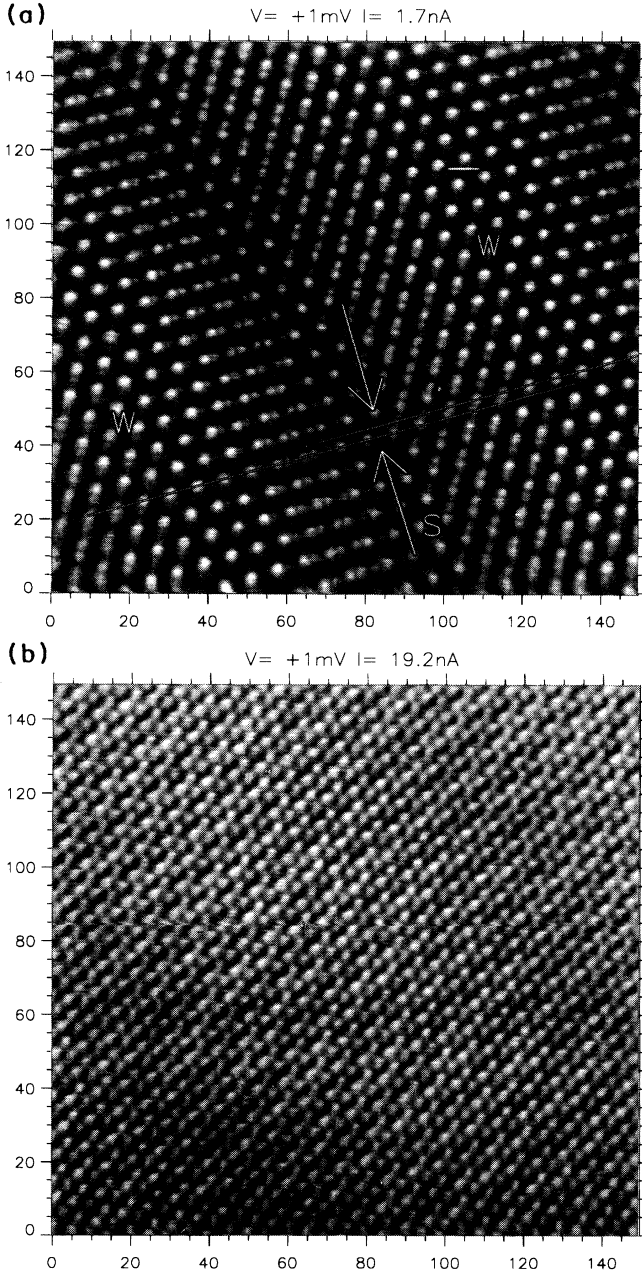

(b)   V= +1mV I= 19.2nA

FIG. 3. High-resolution STM images of the striped incommensurate phase of Pb on Ge(111), (a) acquired at +1-mV sample bias and 1.68-nA tunneling current, (b) same area of the sample imaged at a higher tunneling current.

that each domain wall separates two of the equivalent subdomains of the commensurate reconstruction. It is worth noticing that the units in the middle of the domain walls have a hexagonal symmetry. At a higher tunneling current, the appearance of the domain-wall pattern changes drastically [see Fig. 3(b)]. One now sees a slightly distorted (1×1) pattern and the domain walls are almost invisible. We have shown that it is not possible to relate the maxima in Fig. 3(b) directly to the positions of the Pb atoms, but they can be related to the (1×1) substrate lattice.[19]

We studied systematically the dependence of the incommensurate phase on both the coverage and the annealing temperature. In agreement with domain-wall theory, the distance between the domain walls decreases with increasing coverage, while the width of the domain walls remains constant. We observed a minimum distance between the domain walls of $\sim$130 Å.

The densely packed $\sqrt{3} - \beta$ phase of Pb on Ge(111) is known to undergo a reversible $\sqrt{3} \leftrightarrow (1 \times 1)$ phase transition on heating. This phase transition has been suggested as a possible candidate for a 2D melting process and is still discussed controversely. In agreement with other authors, we observed a jump in the $\sqrt{3} \leftrightarrow (1 \times 1)$ transition temperature close to the saturation coverage of the $\sqrt{3} - \beta$ phase. For coverages below the saturation coverage, the transition temperature is 182 °C and at higher coverage it is 333 °C according to Ref. 13. From the combination of room-temperature STM and RHEED at various temperatures we obtained the following results: The lower transition temperature corresponds to the commensurate $\sqrt{3} - \beta$ phase, while the higher transition temperature can be assigned to the striped incommensurate phase with the minimum domain-wall distance. Heating the SIC very carefully to only slightly above the transition temperature is completely reversible. Heating too much results in a loss of lead from the surface, the transition temperature decreases, and at room temperature either a striped phase with a larger domain-wall distance or a commensurate $\sqrt{3} - \beta$ phase was observed with STM. In this context it should be noticed that several theories of 2D melting connect the melting process with the existence of dislocations or domain walls.[22,23] It is not clear whether the lead desorbs during the annealing or diffuses into 3D lead crystallites, which we sometimes observed in LEED.

B. Pb on Ge: HIC phase

We have observed an incommensurate structure with a hexagonal symmetry as shown in Fig. 4(a). A hexagonal array of indentations that are oriented parallel to the substrate lattice can be seen with a periodicity of $\sim$150 Å. In a closeup of one of the indentations, one again observes a hexagonal pattern which is now rotated 30° with respect to the substrate [Fig. 4(b)]. The periodicity of this structure is $\sim$3.5 Å and corresponds to a 30° rotated Pb(111) layer. The large superstructure can be interpreted as a moiré effect caused by a small mismatch between the substrate and the close-packed rotated Pb(111) layer.[24]

(a)

V= +1.7V I= 4.1nA

[01$\bar{1}$]

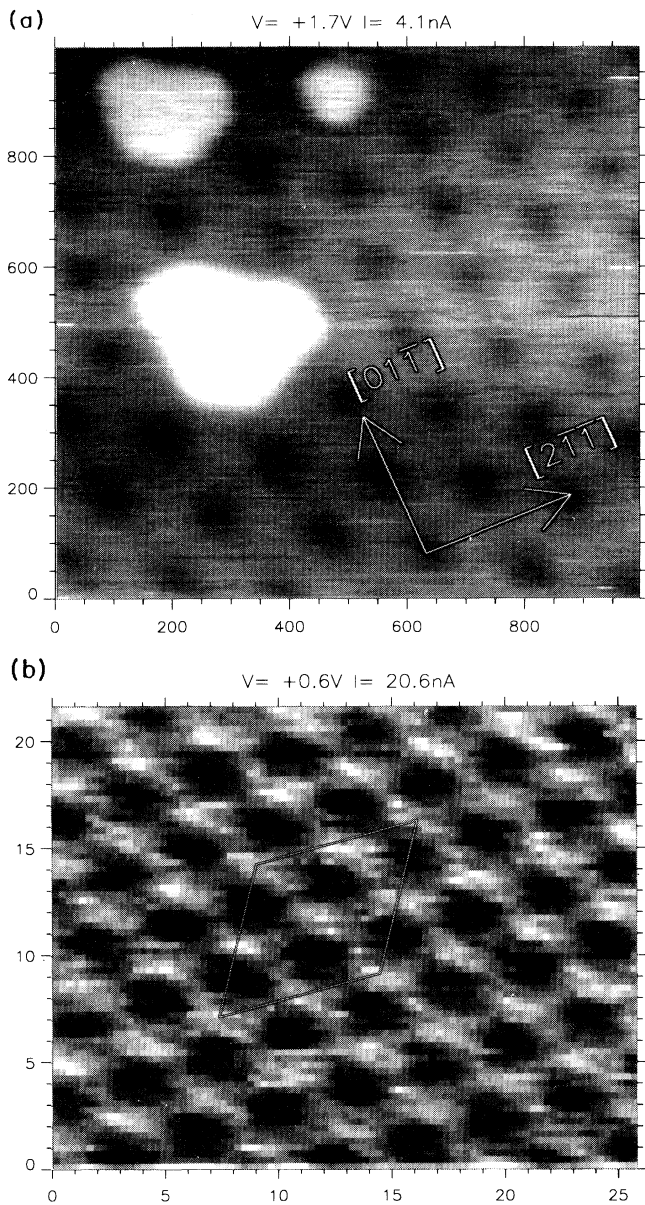[2$\bar{1}$$\bar{1}$]

(b)

V= +0.6V I= 20.6nA

FIG. 4. (a) STM topograph of the hexagonal incommensurate phase of Pb on Ge(111). (b) Closeup of (a). The outlined area corresponds to a $\sqrt{3}$ unit cell.

C. Pb on Si: SIC phase

Pb on Si(111) has been studied with a variety of experimental techniques such as LEED, RHEED, SXRD, and STM. Most work so far has been carried out on the commensurate phases, namely the low-coverage $\sqrt{3}$ reconstruction and the Si(111)(7 × 7)-Pb reconstruction. The low-coverage $\sqrt{3}$ reconstruction was shown to be well described by a simple adatom model with an intermixing of Si and Pb adatoms both located on T_4 sites.[6,25] The (7 × 7)-Pb reconstruction turned out to be metastable and undergoes on heating an irreversible phase transi-

tion either to the dilute $\sqrt{3}$ phase or to the incommensurate closely packed $\sqrt{3}i$ reconstruction depending on the coverage.[26] (It should be mentioned that the $\sqrt{3}i$ phase is also denoted $\sqrt{3} - \alpha$ phase in the literature. Since this notation is inconsistent with the nomenclature for Pb on Ge(111), it will not be used here.) The reason for the occurrence of the Si(111)(7 × 7)-Pb reconstruction seems to be that a considerable amount of energy is needed to fully remove the stacking fault in the (7 × 7) reconstruction of clean Si. If the sample is prepared at room temperature without subsequent annealing, the dimer rows and the partial stacking fault persist underneath the growing Pb layer.

Less work has been performed on the close-packed $\sqrt{3}i$ reconstruction. Several authors reported missing or very weak 1/3-order spots in the LEED pattern of this phase. Based on this observation Estrup and Morrison proposed a structural model with four atoms per unit cell, which corresponds to a compressed 30° rotated Pb(111) layer.[18] A similar model has meanwhile been established for the closely related commensurate Ge(111)$\sqrt{3} - \beta$ phase.[9,12] However, Grey et al. showed with SXRD that while the $\sqrt{3} - \beta$ phase of Pb on Ge(111) is usually commensurate, the $\sqrt{3}i$ reconstruction of Pb on Si(111) is incommensurate.[11] The most obvious reason for this incommensurability is the comparatively large mismatch between bulk Pb and Si(111). The Ge(111) substrate requires a compression of the Pb adlayer compared to the Pb bulk value of only ~1%, while Si(111) requires a compression of ~5%, which is apparently too much. The SXRD data of Grey et al. indicate a mean compression of the Pb layer of 2.3% and have been interpreted in terms of a domain-wall model.[11] However, as has been discussed by Weitering et al.,[27] it is not possible in this case to distinguish on the basis of diffraction data alone between a fully relaxed incommensurate structure and a domain-wall phase. In a careful LEED study, Ganz et al. showed that the compression of the Pb adlayer varies with coverage; they determined that the compression changes from 0% to 2.3% with increasing coverage.[6] They also presented STM images for both the uncompressed and the fully compressed phase, which displayed a small corrugation (< 0.1 Å) and a lot of defects on the surface, which made the measurement rather difficult. Ganz et al. interpreted their images in terms of a hexagonal incommensurate phase.

Figure 5(a) is an STM image obtained from the Si(111)$\sqrt{3}i$-Pb phase, which clearly shows a distorted striped incommensurate phase. The commensurate domains are covered with a hexagonal pattern of protrusions, which corresponds to a $(\sqrt{3} \times \sqrt{3})R30°$ superstructure with one maximum per unit cell. The width of the commensurate domains is typically 15–25 Å and the image shows a lot of defects. It turned out to be rather difficult to prepare a defect-free Si(111)$\sqrt{3}i$-Pb surface. The reason for this difficulty is probably the fact that the difference between the annealing temperature required to remove the stacking fault in the Si(7 × 7) reconstruction and the desorption temperature of Pb is quite small. We frequently observed features like the bright triangle in the upper left corner of Fig. 5(a), which corresponds to
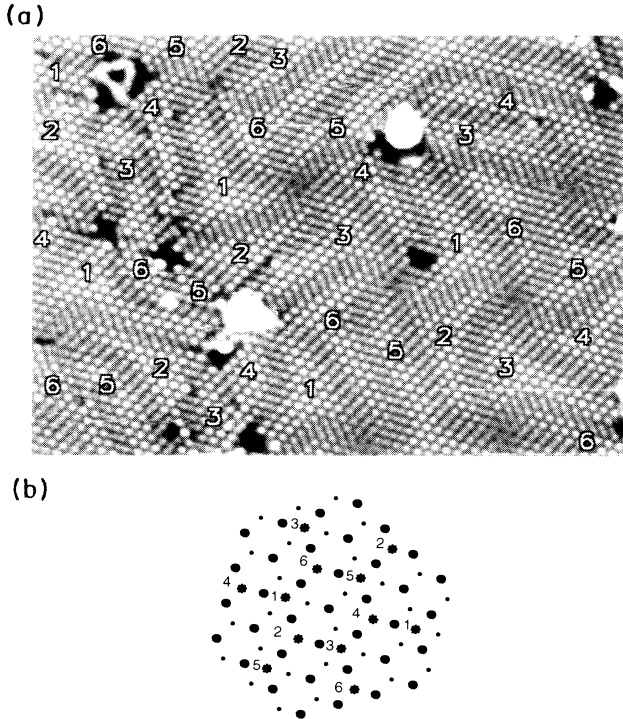
(a)

(b)

FIG. 5. (a) STM topograph acquired at +1.5-V sample bias and 1.6-nA tunneling current from a 360 × 270 Å² area of the striped incommensurate phase of Pb on Si(111). The subdomains are labeled according to (b). (b) The asterisks indicate a possible arrangement of the protrusions in (a) relative to the underlying substrate lattice.

half a Si(111)(7 × 7)-Pb unit cell.

The large number of domain-wall crossings in Fig. 5(a) is either caused by a pinning of the domain walls at defects or by an unfortuitous Pb coverage. On well-prepared surfaces with less defects we observed a homogeneous striped domain-wall pattern with only very few domain-wall crossings. However, we have chosen to show this topograph to discuss a particularly puzzling feature of the domain-wall crossings on the Si(111)$\sqrt{3}i$-Pb reconstruction. In most of the crossings, six domain walls run together while domain-wall theory predicts a maximum of three walls per crossing for a structure with three subdomains ($P = 3$). Mapping the maxima of the STM topograph of Fig. 5(a) onto a (1×1) substrate lattice gives a hint to solving this puzzle. The relative orientation of the protrusions can only be explained assuming the existence of six different commensurate subdomains. Since a $\sqrt{3}$ superstructure only has three subdomains, these six subdomains must be located on two different adsorption sites. A possible arrangement of these six subdomains relative to the substrate is shown in Fig. 5(b). Only the arrangement of the subdomains relative to each other could be determined directly from the STM images of the $\sqrt{3}i$ phase. The registry in Fig. 5(b) has been chosen by analogy to the striped phase of Pb on Ge(111) in which we observed one maximum per $\sqrt{3}$ unit cell on the commensurate domains, which was located on a H_3 site;

at the middle of each domain wall, we observed a hexagonal pattern of protrusions, which were located on T_4 sites. In the case of Pb on Si(111), the energy difference between these two adsorption sites is apparently so small that they are almost equally populated. Furthermore, both types of domains have similar shapes and sizes.

It should be mentioned that the existence of two different occupied adsorption sites (either with hcp or fcc stacking) is a well-known phenomenon for the clean metal surfaces Au(111) and Pt(111). The corresponding domain-wall structures have been studied extensively both experimentally and theoretically.[28–30] However, the domain-wall patterns on the clean metal surfaces differ markedly from the patterns we observed for the Pb-covered semiconductor surfaces.

The special kind of domain walls in the Si(111)$\sqrt{3}i$-Pb phase implies certain rules for the topology of a domain-wall network. According to Fig. 5(b), an oddly labeled domain may only have an evenly labeled neighbor and vice versa. It is important to notice that the resulting domain boundaries are not domain walls in the usual sense since they separate domains that belong to two different adsorption sites. Therefore, they should rather be called *semi-domain-walls* since two of them are needed to separate equivalent subdomains. The width of the commensurate domains of this striped phase was 15–25 Å. The periodicity of the domain-wall pattern, i.e., the average distance between two subdomains on the same adsorption site perpendicular to the domain walls was 45–80 Å. The maximum observed corrugation was 0.5 Å; however, the measured corrugation depended strongly on the condition of the tunneling tip.

High-resolution images of the striped phase also have a very distinctive appearance (see Fig. 6). Instead of one
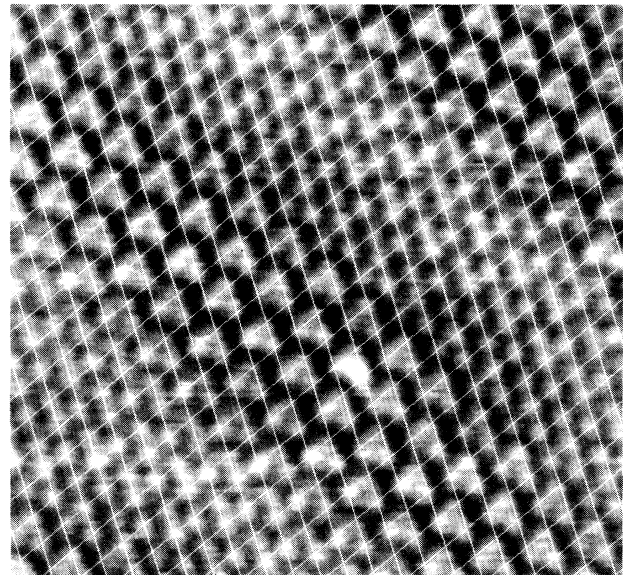

FIG. 6. High-resolution STM image of the striped incommensurate phase of Pb on Si(111) acquired at +0.27-V sample bias and 2.0-nA tunneling current. The superimposed bright lines correspond to a (1×1) lattice.

maximum per $\sqrt{3}$ unit cell, one now sees a more or less distorted (1×1) pattern with a corrugation of ~ 0.25 Å. Usually the protrusions form trimers that often exist in two different 180° rotated orientations. This appearance of the Si(111)$\sqrt{3}i$-Pb phase turned out to be very reproducible for tunneling parameters $|U| < 0.5$ V, $I > 1$ nA. For larger sample bias we usually observed only one protrusion per $\sqrt{3}$ unit cell.

D. Pb on Si: HIC phase

Figure 7(a) also shows a topograph of the Si(111)$\sqrt{3}i$-Pb phase; however, its appearance is quite different from the previously discussed striped phase. The commensurate domains still show one maximum per $\sqrt{3}$ unit cell. Although the resolution is poorer, the shape of the protrusions resembles the trimers visible in Fig. 6. The topology of the domain-wall network has changed completely and we now observe some sort of hexagonal incommensurate phase. There are six almost equivale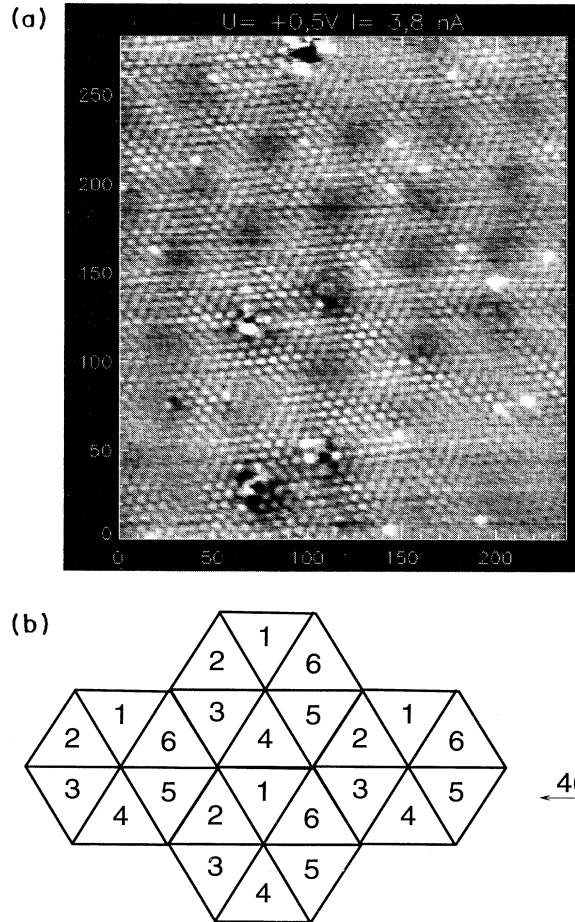nt subdomains on two different adsorption sites. A schematic arrangement of the different subdomains is shown in Fig. 7(b). Again the two adsorption sites seem to be almost equally populated. It is important to note that the domain-wall pattern of the hexagonal incommensurate phase of Pb on Si(111) differs markedly from those previously considered theoretically. There are six semi-domain-walls per wall crossing in the case of Pb on Si(111) compared to three normal domain walls for the ordinary HIC. This leads to a different pattern of crossings — namely, a filled hexagon pattern for Pb on Si(111) and a honeycomb pattern for the conventional HIC and consequently a different density of domain-wall crossings per unit area. Since each domain-wall crossing contributes to the internal energy, the higher density of domain-wall crossings will also increase the total energy of the system.

For the hexagonal phase of Pb on Si(111), we usually found lots of defects as for the striped phase. However, on the hexagonal phase they seem to have a smaller influence on the domain-wall pattern. Hence, we were able to determine the periodicity of the domain-wall pattern quite accurately to be 46 Å, which is smaller than the corresponding value for the striped phase of 50–80 Å. Using x-ray diffraction, Grey et al. determined the periodicity of the $\sqrt{3}i$ phase to be 85 Å.[11] From the peak width of the satellite spots they calculated a lateral coherence length of 130 Å. Since they observed the $\sqrt{3}i$ spots in coexistence with 3D Pb crystallite reflections, they concluded that they had measured a fully compressed Pb layer. By comparison with our STM results, the short coherence length and the large periodicity both indicate that they measured the striped incommensurate phase.

E. Pb on Si: RHEED, LEED, and STM

We were able to obtain additional information about the different phases of Pb on Si(111) from a careful comparison of STM, LEED, and RHEED data measured on the same samples. In Fig. 8, LEED patterns of the striped and the hexagonal phase are shown. The arrows indicate the (1,0) spots. The two satellites close to the (1,0) spot are a characteristic of the striped phase. The (1/3,1/3) spots are split for both phases, but the spot

FIG. 7. (a) STM topograph of the hexagonal incommensurate phase of Pb on Si(111). (b) Schematic arrangement of the domains in (a).
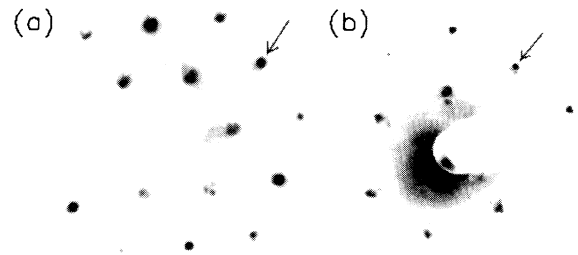

FIG. 8. LEED patterns of the incommensurate phases of Pb on Si(111). (a) HIC 84.5 eV, (b) SIC 30.5 eV. The first Brillouin zone has the same size in both images since they have been scaled appropriately. The arrows indicate the (1,0) spots.
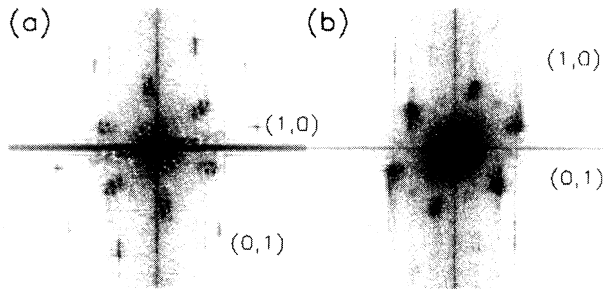
FIG. 9. 2D Fourier transforms of STM topographs of the incommensurate phases of Pb on Si(111). (a) HIC, and (b) SIC.

splitting for the hexagonal phase is much larger than for the striped phase. The spots of the striped phase are less sharp and an additional characteristic satellite can be observed, which is shifted from (1/3,1/3) towards (0,0). A comparison between these LEED patterns and 2D Fourier transforms of STM images of the same samples (Fig. 9) gives a good agreement for the features in the vicinity of the (1/3,1/3) spot. The two phases also can be distinguished in RHEED as shown in Fig. 10. The hexagonal phase displays a strong vertical splitting of all streaks. For the striped phase, the vertical splitting is less sharp and an additional horizontal splitting of the (1/3,1/3) and (2/3,2/3) streaks can be seen.

After learning how to identify the two phases unambiguously with all three experimental techniques, we studied the different phases as a function of temperature and Pb coverage. Adding a small amount of Pb to a sample with the hexagonal phase produces a striped phase. Desorbing a small amount of Pb from a striped phase sample by annealing briefly at about $\sim 350\,^\circ$C leads to a hexagonal phase. Therefore, we conclude that there is a reversible coverage-dependent phase transition between a striped and a hexagonal phase. Interestingly such kinds of phase transitions have already been discussed within the framework of the domain-wall theory for CI phase transitions as being due to the contribution of the breathing entropy of the domain-wall pattern of the hexagonal phase to the total free energy of the adsorbate system.[16,37]

F. Si(111)(1 × 1)-Pb

The reversible temperature-dependent $\sqrt{3}\leftrightarrow(1\times 1)$ phase transition of the densely packed $\sqrt{3}-\beta$ phase of Pb on Ge(111) has attracted considerable attention recently since it may permit a 2D melting process to be investigated experimentally.[31-33] The phase diagram of Pb on Si(111) shows a rather similar phase transition which, however, has been less thoroughly investigated.[26] The transition temperature in both of these systems shows a pronounced coverage dependence. For Pb on Si(111), it was shown to be possible to reduce the transition temperature well below room temperature by carefully desorbing Pb from the fully compressed $\sqrt{3}i$ phase.[34] This opens up the possibility of studying the "high-temperature" Si(111)(1 × 1)-Pb phase with our room-temperature STM.

Figure 11 shows a (1 × 1) reconstructed domain in coexistence with the commensurate dilute $\sqrt{3}$ reconstruction. The latter has been shown to be well described by a simple adatom model with an intermixing of Pb and Si adatoms both located on T_4 sites in analogy with the $\sqrt{3}-\alpha$ phase of Pb on Ge(111).[6,25] By means of the superimposed (1 × 1) grid, we can determine the registry of the protrusions in the (1 × 1) reconstruction. The small shift of the (1 × 1) grid against the position of the adatoms in the $\sqrt{3}$ reconstruction indicates that the protrusions in the (1 × 1) reconstructed domain are located on T_1 sites. At higher coverages we also observed the (1 × 1) phase in coexistence with a usually rather disordered hexagonal incommensurate phase. Figure 12 shows an STM topograph of a sample with a coverage greater than the saturation coverage of the (1 × 1) phase. In the upper part of the image, a (1 × 1) pattern can be observed, while the lower part shows groups of trimers that correspond to a $\sqrt{3}$ superstructure. It should be kept in mind that the $\sqrt{3}$ pattern with three maxima per unit cell corresponds to a slightly distorted (1 × 1) pattern. Since the protrusions in the (1 × 1) phase are located at T_1 sites, it can be deduced directly from Fig. 11 that the maxima in the $\sqrt{3}$ reconstructed domain are also located close to T_1 sites. Since the striped and the hexagonal phase are closely related it seems likely that the maxima in the high-resolution images of the striped phase are located near T_1 sites. We typically measured a corrugation
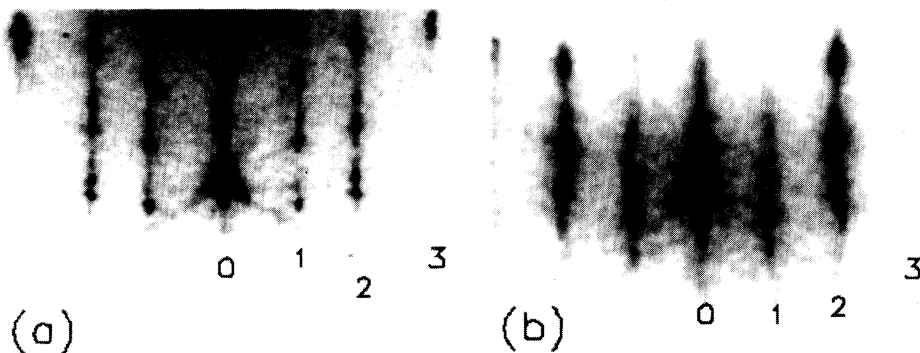

FIG. 10. RHEED patterns (20 keV, [11$\bar{2}$] azimuth) of the incommensurate phases of Pb on Si(111). (a) HIC and (b) SIC. The numbers 0-3 indicate the (0,0) , $(\frac{1}{3},\frac{1}{3})$, $(\frac{2}{3},\frac{2}{3})$, and (1,1) streaks.
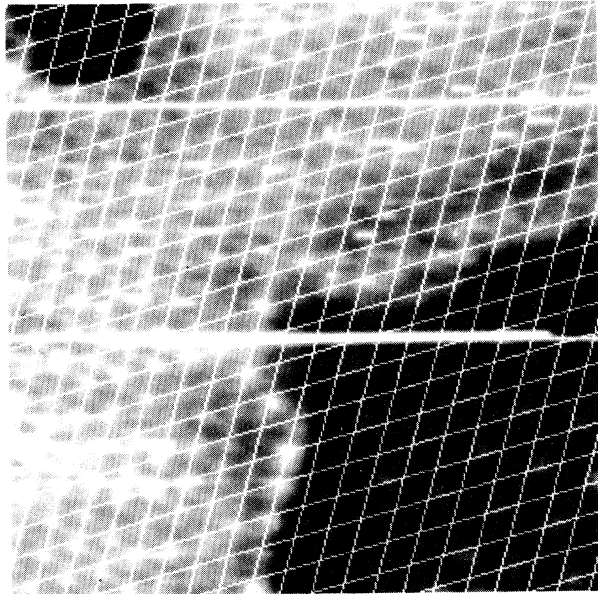
FIG. 11. STM topograph acquired at $+0.88$-V sample bias and 1.3-nA tunneling current from a 66×70 Å^2 area of a Si(111) sample covered with $\sim$0.8-ML Pb. The room-temperature (1×1) phase is in coexistence with the commensurate $\sqrt{3} - \beta$ phase. The superimposed (1×1) lattice has been aligned with the (1×1) phase.
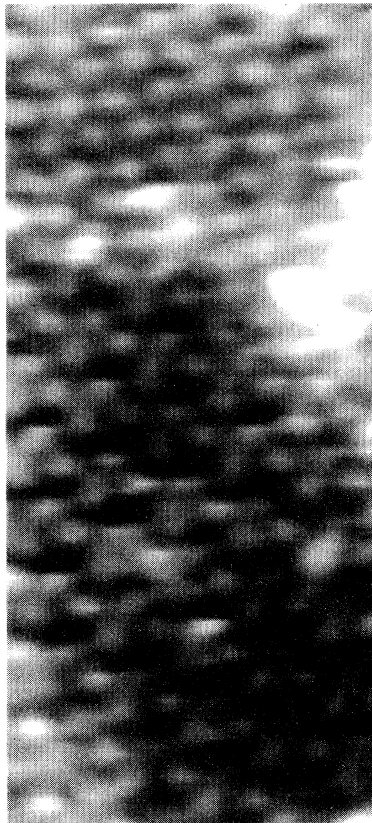

FIG. 12. STM topograph acquired at $+47$-mV sample bias and 1.0-nA tunneling current from a 30×62 Å^2 area of a Si(111) sample covered with $\sim$1.2-ML Pb. A distorted HIC (bottom) is in coexistence with the room-temperature (1×1) phase (top).

on the (1×1) phase of 0.25 Å, which is roughly the same as that in the high-resolution images of the $\sqrt{3}i$ phases.

IV. DISCUSSION

A. Comparison: Pb on Ge(111) and Si(111)

In the previous sections, experimental data on several closely packed 2D structures of Pb on Ge(111) and Si(111) have been presented. The data obtained on the different phases can be explained consistently by assuming that all of these phases are closely related to a $\sqrt{3}$ superstructure with four atoms per unit cell, which corresponds to a slightly compressed 30° rotated Pb(111) layer. Pb on Ge(111) displays, in addition to the commensurate $\sqrt{3} - \beta$ phase, both a striped incommensurate phase and an almost fully relaxed incommensurate phase. The coverage of both of these incommensurate phases is slightly higher than the commensurate value. The commensurate $\sqrt{3} - \beta$ phase requires a 1% compression of the Pb adlayer compared to the bulk value. The moiré pattern of the almost fully relaxed incommensurate phase indicates a compression corresponding to 2.3%.[24] A commensurate $\sqrt{3}$ phase on the Si(111) substrate would require the overlayer to be compressed by 5%. This is apparently too much and consequently no commensurate $\sqrt{3}$ phase of Pb on Si(111) is observed. Hence, we expect the domain walls of Pb on Si(111) to have a Pb density below the commensurate value. Experimentally we observed a reversible coverage-dependent phase transition between the HIC and the SIC. From the typical distance between the semi-domain-walls in the SIC of 25 Å, one can calculate the semi-domain-wall density to be 0.04 Å^{-1}. The periodicity of the HIC of 46 Å corresponds to a semi-domain-wall density of 0.13 Å^{-1}. Since we observed the HIC at a lower coverage than the SIC, we have confirmed experimentally that the domain-wall density decreases with increasing coverage, i.e., the domain walls of Pb on Si(111) have a Pb density below the commensurate value. This illustrates a major difference between the incommensurate phases on the two substrates. The reason for the incommensurability of Pb on Ge(111) is the compression of the adlayer at a Pb coverage above the commensurate value while for Pb on Si(111) the incommensurability is caused by the large intrinsic misfit between the substrate and the adsorbate.

B. Structure of the domain walls

To calculate the coverage of the various densely packed phases from the domain-wall pattern, we have to make assumptions about the atomic structure of the domain walls taking into account the structure of the individual unit cells. Figure 13(a) shows a schematic structural model of a single $\sqrt{3}$ unit cell. Only one Pb atom per unit cell is located on a high symmetry site (H_3) while the other three are placed in bridge positions between T_1 and T_4 sites. The dotted line represents the direction of a domain wall. In the domain-wall theory for CI phase transitions, each domain wall introduces a phase shift,
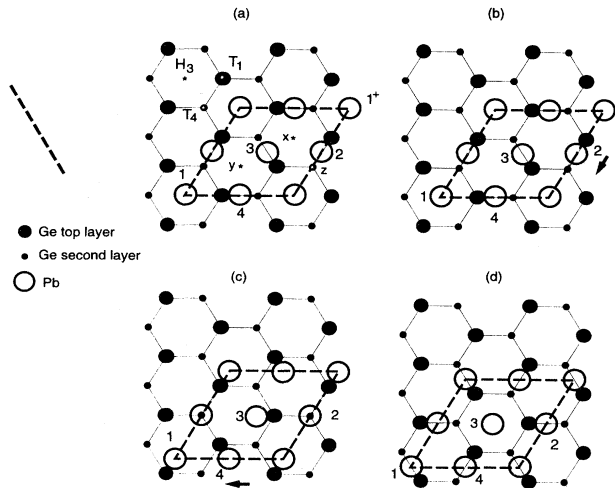
FIG. 13. (a) Schematic model for the closely packed structures of Pb on Ge(111) and Si(111). The Pb atoms are labeled with numbers while adsorption sites are labeled with small letters. The three high symmetry adsorption sites T_1, T_4, and H_3 are also shown. The shift of the individual unit cells introduced by a domain wall of Pb on Ge(111) is illustrated in (b–d): (b) on the left-hand side of the domain wall, (c) in the middle of the domain wall, and (d) on the right-hand side of the domain wall. The arrows indicate the direction of the compression and the dashed line indicates the direction of the domain wall.

FIG. 14. High-resolution STM image of Ge(111)SIC-Pb. The three highlighted $\sqrt{3}$ unit cells correspond to Fig. 13(b–d).

which corresponds to one or two substrate lattice constants for a $\sqrt{3}$ superstructure on a hexagonal substrate. For a heavy domain wall, the Pb atom "1^+" — which is equivalent to the atom "1" — would be shifted to the H_3 position at "x". For a light domain wall, the atoms would shift in the opposite direction. The structural model for the single unit cell shown in Fig. 13(a) opens up the possibility of a different kind of domain wall with a Pb density above the commensurate value. Instead of the Pb atom "1^+" shifting to "x," the Pb atom "3" can shift to its neighboring H_3 site "y." Thus, the atoms "3" and "1" have exchanged their roles. The atom "3" is now located on the H_3 site while all the other atoms are located on a bridge site between T_1 and T_4 positions. To explain the hexagonal feature in the middle of each semi-domain-wall (see Fig. 3) we have to split the shift into two parts. First, the Pb atom "2" will shift to the neighboring T_4 site "z." This shift is indicated by the arrow in Fig. 13(b). The resulting configuration [see Fig. 13(c)] closely resembles the original model for the commensurate β phase except that the high symmetry site is now the T_4 position and the bridge atoms are now located between T_1 and H_3 sites. In a second step, the atom "3" shifts to the neighboring H_3 site "y" and we end up with the configuration shown in Fig. 13(d).

This model agrees very well with our high-resolution STM topographs. First, the phase shift between two neighboring domains agrees with experiment and second we can compare the model with a high-resolution image of a domain wall. The three $\sqrt{3}$ unit cells outlined in the
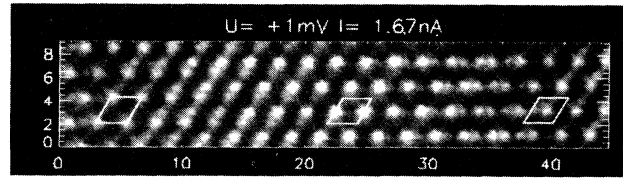
STM image shown in Fig. 14 correspond to the structural models shown in Figs. 13(b)–13(d). We find good agreement if we assume that the protrusions in the STM images are located at the positions of the Pb atoms on high symmetry sites. The STM topograph in Fig. 14 shows in the unit cell on the left-hand side only protrusions at the corners of the unit cell. These correspond to the corner H_3 sites in Fig. 13(b). Between the first two unit cells in Fig. 14 an additional protrusion appears, which is located at the T_4 site labeled "z" in Fig. 13(a). For the middle unit cell in the STM topograph, the protrusions at the corners of the unit cell have almost completely disappeared. In the structural model [Fig. 13(c)], the corresponding Pb atom "1" has moved away from its high symmetry site and is now located on a bridge site between H_3 and T_1 and is, therefore, equivalent to atom "4." In Fig. 13(c) only atom "2" is located on a high symmetry site. The position of this atom agrees with the position of the protrusions in the outlined $\sqrt{3}$ unit cell in the middle of Fig. 14. Between the two unit cells on the right-hand side of Fig. 14, one observes an increasing signal in the center of each unit cell. This signal is presumably related to Pb atom "3," which shifts to the high symmetry H_3 site labeled "y." In Fig. 13(d), only atom "3" is located on a high symmetry site while all the other atoms sit on equivalent bridge positions. Accordingly, the STM image displays a single protrusion in the center of the unit cell.

It is remarkable that the shift introduced by a domain wall described by this new model corresponds only to $-\frac{1}{2}a$ where a is the substrate lattice constant, whereas from domain-wall theory one would expect a shift corresponding to Na with an integer N. The reason for this discrepancy is the fact that the atoms labeled 1 and 3 exchange their roles while going from Fig. 13(b) to Fig. 13(d).

It is straightforward to work out an analogous structural model for the domain walls of Pb on Si(111). In this case, as we have shown above, the domain walls have a Pb density below the commensurate value. Hence, we assume for these light semi-domain-walls a phase shift corresponding to $+\frac{1}{2}a$, i.e., that according to Fig. 13(a) the Pb atom labeled "3" shifts to the neighboring H_3 site labeled "x." Again we split the shift into two steps. First Pb atom "4" shifts to the neighboring T_4 site and then Pb atom "3" shifts to the H_3 site "x." As is the case for the heavy semi-domain-walls, we have two closely related kinds of structures both with one atom per $\sqrt{3}$ unit cell located on a high symmetry site (either H_3 or T_4) while

the other three atoms are placed in bridge positions (between T_1 and T_4, or T_1 and H_3). The energy difference between these two structures is rather small in the case of Pb on Si since both configurations seem to occur with the same probability and there are no differences in either the size or the shape of the corresponding domains.

C. Coverage determination

The actual coverage of the samples can be calculated directly from the periodicity of the different domain-wall patterns (see Table I) since we have established a detailed structural model for the domain walls. For all the different structures, the resulting Pb density is higher than that of a Pb(111) bulk layer. The average compression of the different domain-wall structures compared to the Pb bulk value varies between 1.0% and 3.9% (see Table I). Ganz et al. postulated on the basis of their LEED results for Pb on Si(111) the existence of an uncompressed incommensurate Pb layer.[6] However, we found that reducing the coverage on an HIC sample gave rise to a $\sqrt{3}i \leftrightarrow (1 \times 1)$ phase transition.

The various high-resolution STM images show differences between the closely packed Pb layers on the two different substrates. On the commensurate domains of Pb on Ge(111), we observed with the STM patterns with one, three, or four protrusions per $\sqrt{3}$ unit cell depending on the tunneling parameters; on Pb on Si(111), we only observed patterns with one or three maxima per unit cell. Since the geometrical structures of the two systems are rather similar, the discrepancy can be attributed to differences in the electronic structure. This interpretation is supported by recent photoemission data.[35,36] The STM images of Pb on Si(111) with three maxima per unit cell (see Fig. 6), however, seem to be quite similar to the corresponding images on Ge substrates [see Fig. 3(b)]. In this context it is worth looking back to Fig. 6, which shows a high-resolution image of the SIC of Pb on Si(111). The highlighted lines show how this STM topograph can be placed unambiguously over a (1×1) substrate lattice. It can be seen that each protrusion in the STM image is related to a (1×1) lattice point, i.e., the density of the protrusions in the STM image corresponds exactly to 1 ML. For both of the systems, Pb on Ge(111) and Si(111), we have demonstrated that the domain-wall density varies with the Pb coverage. This implies — in agreement with CI phase transition theory — that the

Pb density in the domain walls is different from the commensurate value. However, the trimer patterns of protrusions in some of the STM images of Ge(111)SIC-Pb [see Fig. 3(b)] and all of the high-resolution images of Si(111)$\sqrt{3}i$-Pb (see Fig. 6) correspond to a density of protrusions of exactly 1 ML for a range of Pb coverages. Therefore, this observation excludes the possibility that the protrusions in the STM images correspond directly to the Pb atoms. On the other hand, the periodicity of the substrate lattice corresponds exactly to a coverage of 1 ML. Therefore, we conclude that the electron density, which is measured by the STM in this case, is associated with the substrate rather than the adsorbate lattice. The interaction between the substrate and the adsorbate leads to a slightly distorted (1×1) pattern, however, the adsorbate is not imaged directly.

D. Si(111)(1 × 1)-Pb

Additional information in this context can be gained from a comparison with the (1×1) phases. Our topographs of the (1×1) phase of Pb on Si(111) are very similar to images of the high-temperature (1×1) phase of Pb on Ge(111) measured by Hwang and Golovchenko.[33] Both systems show a (1×1) pattern located on T_1 sites. Hwang and Golovchenko have studied the $(1 \times 1) \leftrightarrow \sqrt{3}$ transition of Pb on Ge(111) as a function of temperature while we investigated the $(1 \times 1) \leftrightarrow \sqrt{3}i$ transition of Pb on Si(111) as a function of Pb coverage. Since the transition temperature changes with coverage the results are rather similar. Close to the transition point, (1×1) patterns and fluctuating patches of trimers coexist (see Fig. 12, compare with Ref. 33). Since trimer patterns obtained on the densely packed phases of Pb on Si(111) and Ge(111) originate rather from the substrate than the adsorbate, we conclude that neither the (1×1) pattern nor the patches of trimers correspond directly to the location of Pb atoms.

It seems possible that the (1×1) pattern is the result of an averaging process since the atomic motions in a 2D liquid should be much faster than the measuring process. This idea is supported by molecular-dynamics simulations as well as x-ray standing wave measurements for Pb on Ge(111), which both determined very large in-plane vibrational amplitudes for the Pb atoms.[31,32] It should be noted that the coverage-dependent $\sqrt{3}i \leftrightarrow (1 \times 1)$ phase transition takes place between two structures, which both

TABLE I. Comparison between the various closely packed phases of Pb on Ge(111) and Si(111). (Note: the coverage values are for two different substrates.)

	$\rho \times cm^2/10^{14}$ atoms	Mean compression	Θ/ML
Pb(111)	9.43	0.0%	
Pb/Si HIC	9.62	1.0%	1.229
Pb/Ge $\sqrt{3} - \beta$	9.63	1.1%	1.333
Pb/Ge SIC$_{max}$	9.78	1.8%	1.354
Pb/Ge(111) HIC	9.89	2.4%	1.370
Pb/Si SIC	10.05–10.18	(3.2–3.9)%	1.28–1.30
4/3 ML on Si(111)	10.44	5%	1.333

show one protrusion per (1×1) unit cell in the STM images. Since one cannot have a coverage-dependent phase transition between two phases with the same coverage, it is almost self-evident that the observed protrusions cannot be related to individual Pb atoms. In agreement with recent x-ray standing wave measurements,[32] the molecular-dynamics simulations of the high-temperature (1×1) phase of Pb on Ge(111) by Ancilotto *et al.*[31] predicted a strong correlation between the substrate and the highly mobile adsorbate, resulting in preferential residence sites for the Pb atoms. These preferential sites probably correspond to the (1×1) pattern of protrusions visible in the STM images.

E. Coverage and temperature dependence

The information obtained on the phase transitions between the various closely packed structures of Pb on Ge(111) and Si(111) can be summarized in the schematic

phase diagrams shown in Fig. 15. The various coverages have been taken from Table I while the temperatures have been taken from Refs. 13 and 26. It is interesting to compare these phase diagrams with simple theoretical considerations within the framework of domain-wall theory. Villain and Gordon noticed that in a HIC a single domain can "breath," i.e., change its size, without changing the total length of the domain walls, or the number of domain-wall intersections.[37] Since the latter two terms dominate the internal energy of the system the breathing allows the internal energy to remain constant.[17,37] There is no equivalent effect for a striped incommensurate phase. As shown by Bak *et al.* for $T = 0$ the sign of the energy contribution of the domain-wall crossings determines whether a striped or a hexagonal incommensurate phase develops.[17] For $T > 0$, the breathing entropy might stabilize the HIC over a certain coverage range even for a positive domain-wall crossing energy. In the theoretical phase diagrams, the HIC is placed between the commensurate phase and the SIC.[16]

At first sight it might seem surprising that for Pb on Ge(111) we determined a higher coverage for the HIC than for the SIC. A closer inspection of the various STM images indicates, however, that the hexagonal incommensurate phase is an almost fully relaxed incommensurate phase rather than a domain-wall phase. This interpretation is also supported theoretically since domain-wall theory is only applicable for small lattice mismatch. For an increased lattice mismatch theory predicts a phase transition from a domain-wall phase to a relaxed incommensurate phase.[16]

The case of Pb on Si(111) is more difficult to explain. The STM topographs clearly show domain-wall structures for both the SIC and the HIC. In contradiction to theory, we observe an SIC→HIC phase transition with increasing domain-wall density. Since this is exactly the opposite of what one would expect theoretically, this point clearly needs further investigation.

Another interesting aspect of the schematic phase diagram in Fig. 15 is the temperature dependence of the $\sqrt{3} \leftrightarrow (1 \times 1)$ phase transition. In both cases the transition temperature decreases with decreasing coverage. As shown above for Pb on Si(111) a decrease in the coverage implies an increase in the domain-wall density. Therefore, we conclude that in this case the domain walls destabilize the $\sqrt{3}$ structure. In the case of Pb on Ge(111) it is just the other way around; the commensurate phase has a lower transition temperature than the striped domain-wall phase. Hence, in this case the domain walls seem to stabilize the $\sqrt{3}$ structure. The discrepancy can be explained if we assume that the $\sqrt{3} \leftrightarrow (1 \times 1)$ transition is indeed some kind of melting process. A useful definition of a liquid in this context is its inability to resist shear stress.[23] Shearing a domain-wall structure requires the formation of additional domain-wall intersections. Since the free energy of a domain-wall intersection is negative for a HIC and positive for a SIC it seems reasonable that the melting temperature will be increased for a SIC and reduced for a HIC compared to the value for the commensurate phase. However, the reason for the existence of the HIC phase of Pb on Si(111) remains unclear.

FIG. 15. Schematic phase diagrams of the closely packed phases of Pb on Ge(111) (a) and Si(111) (b). The temperatures were taken from Refs. 13 and 26. The coverages were calculated from the domain walls using the structural model in Fig. 13. The HIC of Pb on Ge is metastable while the commensurate $\sqrt{3}$ phase of Pb on Si(111) could not be observed and is only indicated in the diagram for comparison.

F. Influence of defects

Our samples of the close-packed phases of Pb on Si(111) usually displayed a lot of defects [typically 150 per (1000 Å)²] in the STM images. The defect density depends both on the quality of the clean substrate and on the annealing procedure after Pb deposition. Very careful annealing of the Pb-covered Si(111) was required to completely remove the partial stacking fault of the substrate without desorbing too much Pb. Our best Pb on Si(111) samples had a point-defect density of 30 per (1000 Å)² while our best Pb on Ge(111) samples had a defect density of < 10 per (1000 Å)². To study the influence of the defects on the domain-wall patterns, we compared defect-rich and well-prepared samples at different coverages. We found that the various phases and phase transitions were not sensitive to the defect density. The only effect we observed was that a higher defect density leads to an increased number of domain-wall crossings in the striped phases. This is probably caused by a pinning of the domain walls at the defects.

V. CONCLUSIONS

We have examined in detail the various densely packed room-temperature phases of Pb on Ge(111) and Si(111). Pb on Ge(111) displays a commensurate $\sqrt{3} - \beta$ phase,

a SIC phase, and a metastable almost fully relaxed incommensurate phase with hexagonal symmetry. Depending on the coverage, Pb on Si(111) displays a (1×1), a HIC, and a SIC phase. All the observed phases can be explained by a structural model, which corresponds to a slightly compressed 30° rotated Pb(111) layer located above an ideally terminated semiconductor surface. Based on this model for the commensurate units, we developed an atomic model for the different domain-wall structures. We presented high-resolution STM images for all the different room-temperature phases and related these results to temperature-dependent RHEED and LEED measurements. In this way we were able to establish schematic phase diagrams for both adsorbate systems. The formation of the SIC phase in the case of Pb on Ge leads to an increase in the $\sqrt{3} \leftrightarrow (1 \times 1)$ transition temperature. For Pb on Si(111) the transition from the SIC to the HIC — which is also coupled with an increase in the domain-wall density — gives rise to a reduction of the transition temperature.

ACKNOWLEDGMENTS

[1] See, e.g., the series *Phase Transitions and Critical Phenomena*, edited by C. Domb and J. L. Lebowitz (Academic Press, London).

[2] *Ordering in Two Dimensions*, edited by S. K. Sinha (North-Holland, Amsterdam, 1980).

[3] A. G. Naumovets, Contemp. Phys. **30**, 187 (1989)

[4] See, e.g., K. Kern and G. Comsa, in *Chemistry and Physics of Solid Surfaces*, edited by R. Vanselow and R. Howe (Springer, Berlin, 1988), Vol. VII.

[5] E. Ganz, F. Xiong, I.-S. Hwang, and J. Golovchenko, Phys. Rev. B **43**, 7316 (1991).

[6] E. Ganz, I.-S. Hwang, F. Xiong, S. K. Theiss, and J. Golovchenko, Surf. Sci. **257**, 259 (1991).

[7] M. J. Hadley, S. P. Tear, and T. N. Doust, J. Phys. Condens. Matter **3**, 277 (1991); Appl. Surf. Sci. **56-58**, 137 (1992).

[8] L. Seehofer, G. Falkenberg, and R. L. Johnson, Surf. Sci. **290**, 15 (1993).

[9] R. Feidenhans'l, J. S. Pedersen, M. Nielsen, F. Grey, and R. L. Johnson, Surf. Sci. **178**, 927 (1986); **189/190**, 1047 (1987).

[10] F. Grey, Ph.D. thesis, Copenhagen University, 1988.

[11] F. Grey, R. Feidenhans'l, M. Nielsen, and R. L. Johnson, J. Phys. (Paris) Colloq. **50**, C7-181 (1989).

[12] H. Huang, C. M. Wei, H. Li, B. P. Tonner, and S. Y. Tong, Phys. Rev. Lett. **62**, 559 (1989).

[13] T. Ichikawa, Solid State Commun. **49**, 59 (1984).

[14] F. Grey, R. Feidenhans'l, J. Skov Pedersen, M. Nielsen, and

R. L. Johnson, Phys. Rev. B **41**, 9519 (1990).

[15] F. C. Frank and J. H. Van der Merwe, Proc. R. Soc. London Ser. A **198**, 205 (1949).

[16] P. Bak, Rep. Prog. Phys. **45**, 587 (1982).

[17] P. Bak, D. Mukamel, J. Villain, and K. Wentorska, Phys. Rev. B **19**, 1610 (1979).

[18] P. J. Estrup and J. Morrison, Surf. Sci. **2**, 465 (1964).

[19] L. Seehofer, G. Falkenberg, D. Daboul, and R. L. Johnson, Surf. Sci. **314**, L879 (1994); L. Seehofer, Ph.D. thesis, Universität Hamburg, 1993.

[20] V. L. Pokrovsky, Helv. Phys. Acta **56**, 677 (1983).

[21] V. L. Pokrovsky, J. Phys. **42**, 761 (1981).

[22] J. M. Kosterlitz and D. J. Thouless, J. Phys. C **6**, 1181 (1973).

[23] W. F. Brinkman, D. S. Fisher, and D. E. Moncton, Science **217**, 693 (1982).

[24] L. Seehofer, D. Daboul, G. Falkenberg, and R. L. Johnson, Surf. Sci. **307-309**, 698 (1994).

[25] C. J. Karlsson, E. Landemark, Y.-C. Chao, and R. I. G. Uhrberg, Phys. Rev. B **45**, 6321 (1992).

[26] H. Yaguchi, S. Baba, and A. Kinbaara, Appl. Surf. Sci. **33/34**, 75 (1988).

[27] H. H. Weitering, D. R. Heslinga, and T. Hibma, Phys. Rev. B **45**, 5991 (1992).

[28] M. El-Batnouny, S. Burdick, K. M. Martini, and P. Stancioff, Phys. Rev. Lett. **58**, 2762 (1987).

[29] A. R. Sandy, S. G. J. Mochrie, D. M. Zehner, G. Grübel, K. G. Huang, and D. Gibbs, Phys. Rev. Lett. **68**, 2192 (1992).

[30] S. Narasimhan and D. Vanderbilt, Phys. Rev. Lett. **69**, 1564 (1992).

[31] F. Ancilotto, A. Selloni, and R. Car, Phys. Rev. Lett. **71**, 3685 (1993).

[32] G. E. Franklin, M. J. Bedzyk, J. C. Woicik, C. Liu, J. R. Patel, and J. A. Golovchenko, Phys. Rev. B **51**, 2440 (1995).

[33] I.-S. Hwang and J. Golovchenko, Phys. Rev. Lett. **71**, 255 (1993).

[34] R. Feidenhans'l (private communication).

[35] J. A. Carlisle, T. Miller, and T.-C. Chiang, Phys. Rev. B **45**, 3400 (1992).

[36] J. A. Carlisle, T. Miller, and T.-C. Chiang, Phys. Rev. B **47**, 10 342 (1993).

[37] J. Villain and M. B. Gordon, Surf. Sci. **125**, 1 (1983).
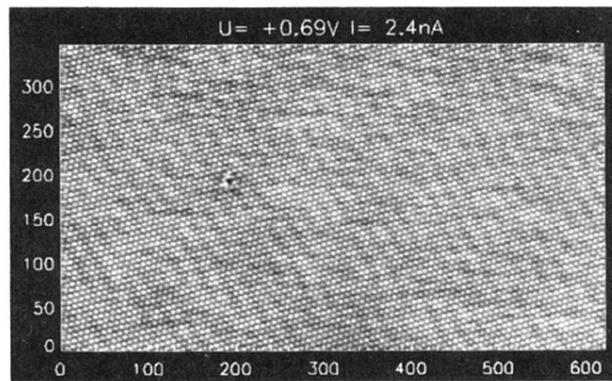
FIG. 1. STM topograph of the commensurate Ge(111)$\sqrt{3} - \beta$-Pb phase.

FIG. 10. RHEED patterns (20 keV, $[11\bar{2}]$ azimuth) of the incommensurate phases of Pb on Si(111). (a) HIC and (b) SIC. The numbers 0–3 indicate the $(0,0)$, $(\frac{1}{3}, \frac{1}{3})$, $(\frac{2}{3}, \frac{2}{3})$, and $(1,1)$ streaks.
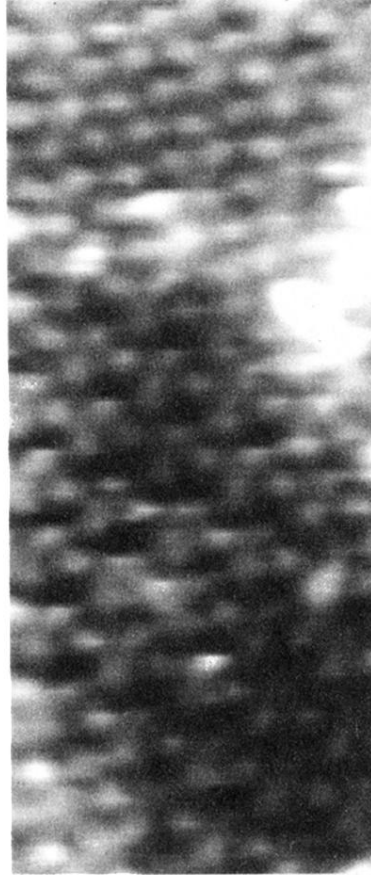
FIG. 11. STM topograph acquired at +0.88-V sample bias and 1.3-nA tunneling current from a 66×70 Å^2 area of a Si(111) sample covered with ~0.8-ML Pb. The room-temperature (1×1) phase is in coexistence with the commensurate $\sqrt{3} - \beta$ phase. The superimposed (1×1) lattice has been aligned with the (1×1) phase.

FIG. 12. STM topograph acquired at +47-mV sample bias and 1.0-nA tunneling current from a 30×62 Å^2 area of a Si(111) sample covered with ~1.2-ML Pb. A distorted HIC (bottom) is in coexistence with the room-temperature (1×1) phase (top).

FIG. 14. High-resolution STM image of Ge(111)SIC-Pb. The three highlighted $\sqrt{3}$ unit cells correspond to Fig. 13(b–d).
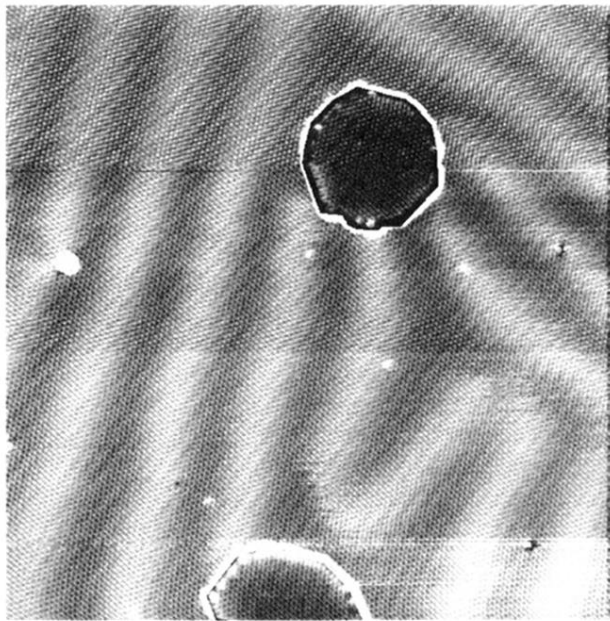
FIG. 2. STM topograph acquired at +1.5-V sample bias and 1.5-nA tunneling current from a 800×800 Å^2 area of the striped incommensurate phase of Pb on Ge(111).
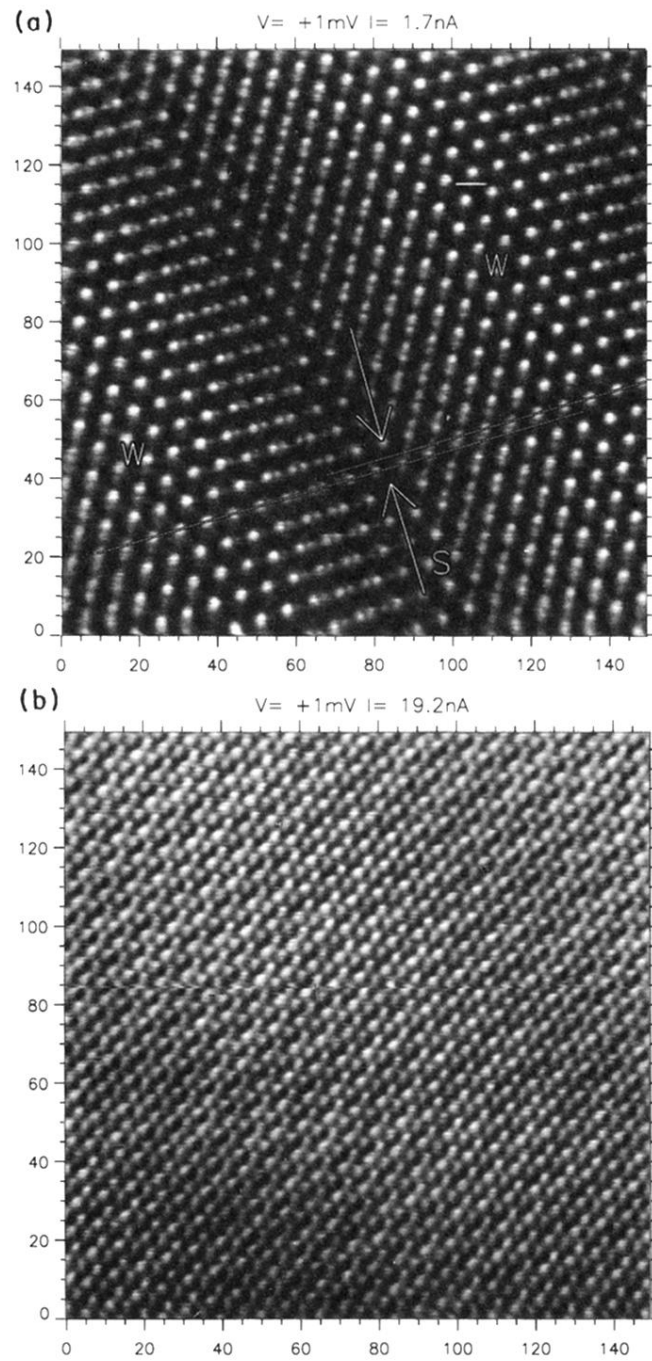
FIG. 3. High-resolution STM images of the striped incommensurate phase of Pb on Ge(111), (a) acquired at +1-mV sample bias and 1.68-nA tunneling current, (b) same area of the sample imaged at a higher tunneling current.
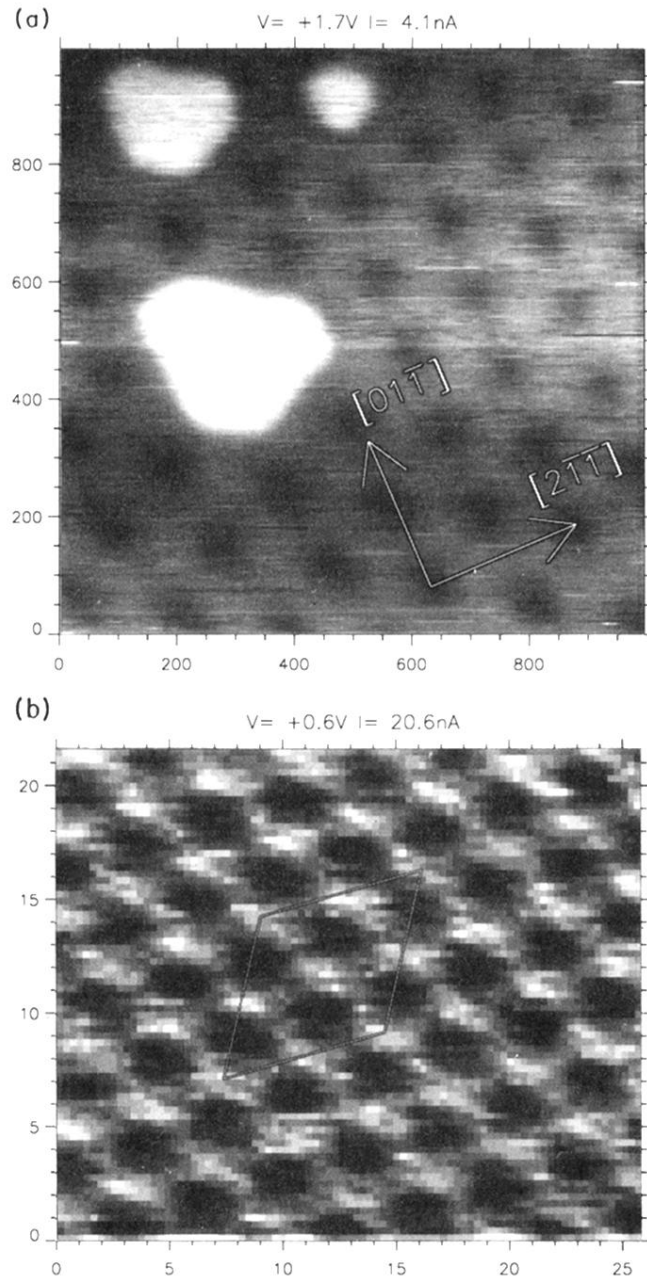
FIG. 4. (a) STM topograph of the hexagonal incommensu-
rate phase of Pb on Ge(111). (b) Closeup of (a). The outlined
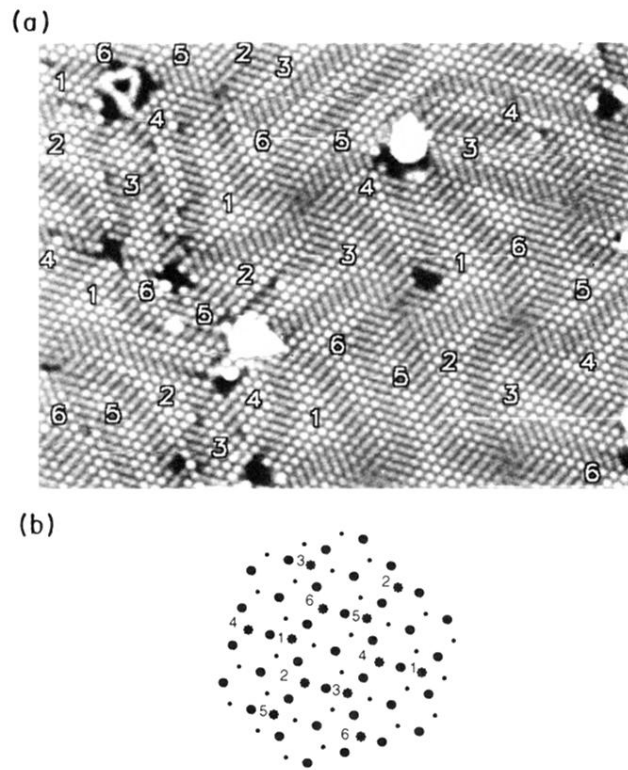area corresponds to a $\sqrt{3}$ unit cell.

(a)

(b)

FIG. 5. (a) STM topograph acquired at +1.5-V sample bias and 1.6-nA tunneling current from a 360×270 Å^2 area of the striped incommensurate phase of Pb on Si(111). The subdomains are labeled according to (b). (b) The asterisks indicate a possible arrangement of the protrusions in (a) relative to the underlying substrate lattice.
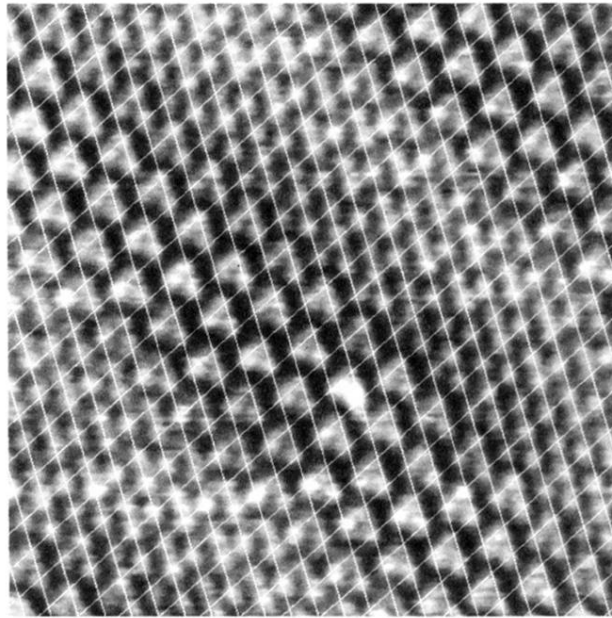
FIG. 6. High-resolution STM image of the striped incommensurate phase of Pb on Si(111) acquired at +0.27-V sample bias and 2.0-nA tunneling current. The superimposed bright lines correspond to a (1×1) lattice.
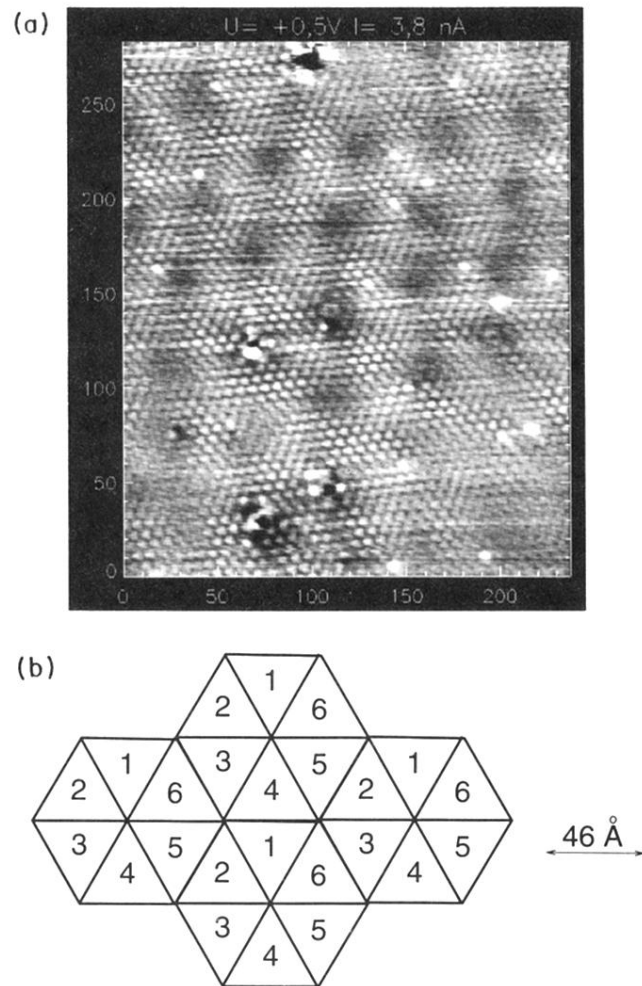
FIG. 7. (a) STM topograph of the hexagonal incommensu-
rate phase of Pb on Si(111). (b) Schematic arrangement of
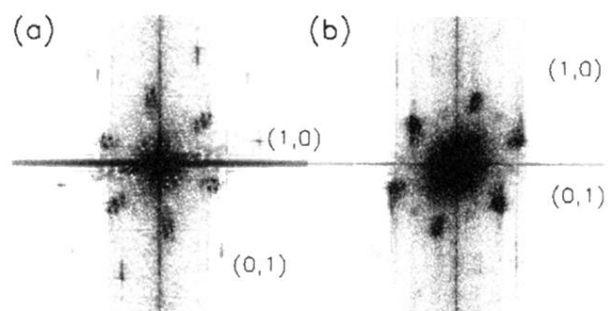the domains in (a).

FIG. 9. 2D Fourier transforms of STM topographs of the incommensurate phases of Pb on Si(111). (a) HIC, and (b) SIC.